

REPORT DOCUMENTATION PAGE

Form Approved
OMB No. 0704-0188

Public reporting burden for this collection of information is estimated to average 1 hour per response, including the time for reviewing instructions, searching existing data sources, gathering and maintaining the data needed, and completing and reviewing this collection of information. Send comments regarding this burden estimate or any other aspect of this collection of information, including suggestions for reducing this burden to Department of Defense, Washington Headquarters Services, Directorate for Information Operations and Reports (0704-0188), 1215 Jefferson Davis Highway, Suite 1204, Arlington, VA 22202-4302. Respondents should be aware that notwithstanding any other provision of law, no person shall be subject to any penalty for failing to comply with a collection of information if it does not display a currently valid OMB control number. **PLEASE DO NOT RETURN YOUR FORM TO THE ABOVE ADDRESS.**

1. REPORT DATE (DD-MM-YYYY) March 2013		2. REPORT TYPE Technical Paper		3. DATES COVERED (From - To) March 2013-May 2013	
4. TITLE AND SUBTITLE POISSON'S RATIO EXTRAPOLATION FROM DIGITAL IMAGE CORRELATION EXPERIMENTS				5a. CONTRACT NUMBER In-House	
				5b. GRANT NUMBER	
				5c. PROGRAM ELEMENT NUMBER	
6. AUTHOR(S) Timothy C. Miller				5d. PROJECT NUMBER	
				5e. TASK NUMBER	
				5f. WORK UNIT NUMBER Q16H	
7. PERFORMING ORGANIZATION NAME(S) AND ADDRESS(ES) Air Force Research Laboratory (AFMC) AFRL/RQRP 10 E. Saturn Blvd. Edwards AFB CA 93524-7680				8. PERFORMING ORGANIZATION REPORT NO.	
9. SPONSORING / MONITORING AGENCY NAME(S) AND ADDRESS(ES) Air Force Research Laboratory (AFMC) AFRL/RQR 5 Pollux Drive Edwards AFB CA 93524-7048				10. SPONSOR/MONITOR'S ACRONYM(S)	
				11. SPONSOR/MONITOR'S REPORT NUMBER(S) AFRL-RQ-ED-TP-2013-154	
12. DISTRIBUTION / AVAILABILITY STATEMENT Distribution A: Approved for Public Release; Distribution Unlimited. PA#13448					
13. SUPPLEMENTARY NOTES Conference paper for the JANNAF S&MBS Conference, Charleston, SC, December 2013.					
14. ABSTRACT Digital image correlation, an optical method that uses speckle patterns to determine surface strains, has been used recently to investigate values for Poisson's ratio in solid propellant specimens. Work was performed on both a double-base and a composite propellant, and results indicate that the method is useful for determination of Poisson's ratio. Details of the experimental procedure, the advantages of the method over current approaches, and the results are described, as well as recommendations for future work.					
15. SUBJECT TERMS					
16. SECURITY CLASSIFICATION OF:			17. LIMITATION OF ABSTRACT	18. NUMBER OF PAGES	19a. NAME OF RESPONSIBLE PERSON Timothy Miller
a. REPORT Unclassified	b. ABSTRACT Unclassified	c. THIS PAGE Unclassified			SAR

POISSON'S RATIO EXTRAPOLATION FROM DIGITAL IMAGE CORRELATION EXPERIMENTS

Timothy C. Miller
Air Force Research Laboratory (RQRP)
10 East Saturn Boulevard, Edwards Air Force Base, California 93524

ABSTRACT

Digital image correlation, an optical method that uses speckle patterns to determine surface strains, has been used recently to investigate values for Poisson's ratio in solid propellant specimens. Work was performed on both a double-base and a composite propellant, and results indicate that the method is useful for determination of Poisson's ratio. Details of the experimental procedure, the advantages of the method over current approaches, and the results are described, as well as recommendations for future work.

INTRODUCTION

Solid rocket propellants, whether composite or double-base, are usually considered incompressible by motor manufacturers. The presumption is that the rubbery elastomer matrix is incompressible and dominates the material behavior, at least for small strains (i.e., prior to dewetting). Also, it is often impractical to measure compressibility. Current rocket laboratory methods measure strains in propellants poorly – this is because the conventional strain measurement methods, such as strain gauges or extensometers, are not optimized for low-stiffness materials such as rubbery elastomers. In addition, many optical methods that were developed for metals measure small strains well but do not work with larger deformations.

For these reasons, it often seems logical to just accept the incompressibility assumption, especially if it seems that the stress analysis is insensitive to the related mechanical properties. However, in many problems, the stress analysis and related failure prediction *does* depend strongly on the assumed level of propellant compressibility – examples include J -integral calculations for flaws near the tip of a star-shaped bore and the stresses in the grain near the case in a center-perforated motor. [1] [2] In such cases, the related linear elastic material parameter, Poisson's ratio, is important but not well characterized – and its assumed value strongly influences the failure predictions.

Since Poisson's ratio is the ratio of two strains from a tensile test, any method of simultaneously measuring these two strains (axial and transverse) could probably be used to determine Poisson's ratio. For a material such as a metal, the ratio of the two strains remains constant throughout the linear elastic regime, and the determination of Poisson's ratio is relatively simple. An ASTM standard describes the use of extensometers (mounted in the two directions) to determine Poisson's ratio, ν_0 , and we have performed a similar procedure with strain gauges. [3]

These methods will not work with rocket propellant, however, since the stiffnesses and strains preclude the use of these measurement methods. For this more complex material behavior, the situation is somewhat complicated. Rocket propellants, like rubbery elastomers, will experience a changing ratio of transverse to axial strains throughout the tensile test. However, in these cases, the linear elastic parameter ν_0 still has some validity and can be determined by extrapolating the value of this ratio back to the undeformed state.

Since Poisson's ratio, the bulk modulus, and Young's modulus are all intimately related, any one of these can be calculated if the other two are known. Currently, some researchers measure compressibility with a special dilatometer and then calculate Poisson's ratio from this data. They do this with either a dilatometer that uses either a gas [4] or a liquid to indirectly measure the change in the volume of a specimen during a tensile test. Then they indirectly determine ν_0 from the bulk modulus and stiffness data. In this work, an alternative method is proposed that measures strains in a more direct fashion – the digital image correlation method is used to get the two strains, and then Poisson's ratio is determined. The use of this more direct method avoids some of the issues that are present when using a dilatometer approach.

EXPERIMENTAL PROCEDURE

Previously we conducted preliminary tests on both a composite propellant and a double-base propellant to determine the best way to use digital image correlation to determine Poisson's ratio. Following these preliminary tests, we conducted a full set of tests on both a double-base and a composite propellant. The double-base propellant was composed of nitroglycerin and nitrocellulose. The composite propellant was a hydroxyl-terminated polybutadiene (HTPB) propellant with an ammonium perchlorate oxidizer. To examine the effects of temperature and strain rate, we used three temperatures (-30°, +20°, and +50° C) and three crosshead speeds (5.08, 50.8, and 508.0 mm/min), with three specimens tested for each of these nine conditions (see Table 1 below).

Table 1 -- Test matrix used for each of the two propellants (The number in each cell indicate the number of tests).

		Crosshead Speed (mm/min)		
		5.08	50.8	508.0
Conditioning Temperature (deg. C)	-30.0	3	3	3
	+20.0	3	3	3
	+50.0	3	3	3

Digital image correlation uses a random speckle pattern on the face of an object to determine surface deformations. Usually this has to be applied. For the double-base propellant, a typical spray-painting technique was used – a white background was speckled with black paint. The perchlorate particles embedded in the matrix of the composite propellant were used as the speckle pattern in the case of the HTPB propellant.

The optical method used here is called three-dimensional digital image correlation and employs two cameras that simultaneously capture pairs of images of the speckled surface to determine strains on the surfaces of specimens. The existing literature [5] describes the mathematics of the method thoroughly – however, for solid propellant tests, there are several noteworthy aspects:

- The method is easy to use. Commercially available systems can capture speckle patterns and analyze the displacements and strains.
- The method is noncontact – the dilatometer chamber and its fluid are no longer necessary.
- Large deformation capability – since the displacement calculations are based on sequential image pairs, large deformations determinations are attainable.
- The method is full-field – this is the most important advantage. Every pixel in the speckled region can have a value determined for each of the in-plane displacement components, which can then be resolved into strains.

The specimen geometry was that of a stress relaxation specimen (101.6 x 12.7 x 12.7 mm). The previous tests indicated that the middle 50.8 mm region in the middle of the specimen gave uniform strains during a tensile test, so this was the speckled region. These specimens were machined using a milling machine and a band saw. Once machined, we glued them to aluminum end tabs. Figure 1 shows typical specimens after surface preparation. Tensile testing consisted of the following steps:

1. Calibration: Calibration involves a calibration target and capturing image pairs of the target in various positions.
2. Temperature conditioning: We conditioned the specimens at the desired test temperature in a separate temperature chamber over several hours and then moved them to the tensile tester and tested them quickly – the tests were always finished within five minutes of removal from the conditioning chamber. This avoids complications with making optical measurements through a temperature chamber window.

3. Tensile testing: This took place in accordance with the test matrix shown in Table 1. For each test condition, multiple trials were conducted. During testing, the capture rate for the imaging system was varied to provide adequate data – this rate varied from 0.5 to 10 image pairs/second.
4. Laser verification: To ensure we were getting accurate data, we used a laser extensometer. This extensometer, aimed at two reflective strips on the backside of some of the specimens, was able to measure axial extension over the same volume as that of the image correlation system. We found the results to be very consistent between the two methods. It then seemed reasonable to conclude that the transverse strain measurements were also accurate.
5. Post-processing: This can take several minutes per test. First, an area of interest is selected using the software. This area can be all or just part of the speckled region. Coordinate directions are selected, and additional parameters such as the mathematical form of the strain tensor are chosen. The software calculates the deformation, then the strains, and then the data is exported into text files.
6. If desired, data is available for every pixel in the area of interest. This amount of data proved unnecessary, however, and for our tests, we sampled uniformly spaced pixels in the area of interest so that 500 or 600 pairs of strain values were determined for each image pair. Using a UNIX script, we took the 500 or so individual values for the strains and averaged them for each point in time, resulting in data that can be used to determine Poisson's ratio.

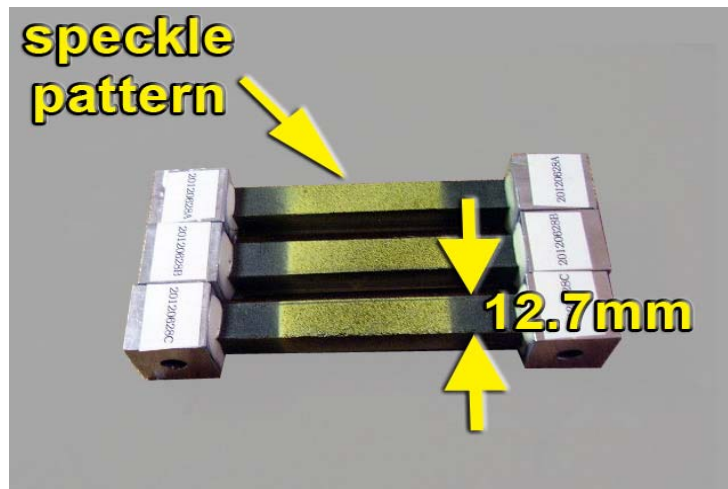


Figure 1-- Double-base propellant specimens glued into aluminum end tabs. Only the middle part of the speckled region was used for property derivation.

RESULTS AND DISCUSSION

For each test, just prior to initiation of crosshead motion, the acquisition portion of the software was used to capture image pairs at a periodic rate that matched the data acquisition rate for the tensile testing machine. An *area of interest* was defined after the test – this was the region over which deformations and strains were to be determined. Next, the software was used to determine the horizontal and vertical deformation components at numerous pixel locations in this area of interest – we limited the number to 500 to 600 values for each displacement component so that postprocessing could be done quickly. The deformations are determined with sub-pixel accuracy. The software features include error norms that describe the correlation accuracy to confirm that the deformation measurements are reasonable. Typical deformation contour plots are shown in Figure 2. Uniform spacing of the bands in the contour plot indicate a uniform strain state, although with experimental data, some deviations are to be expected.

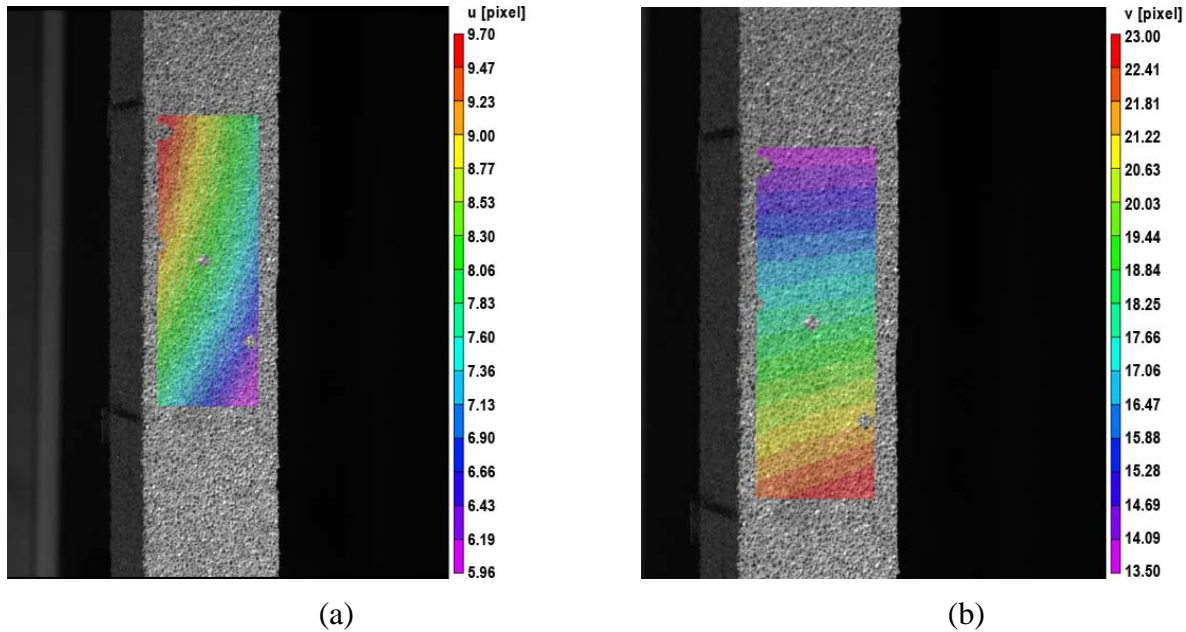


Figure 2 -- Contour maps of deformation components in a typical HTPB propellant specimen with (a) being the horizontal component and (b) being the vertical component. Subsequent differentiation of the deformation components gives strain data.

Once the deformations were determined, the corresponding strain components were determined and the ratio of the two strains was calculated for each image pair. At each acquisition time, the strain values represent an averaging over the whole area of interest, with 500 or 600 values used in each of the averages. For a uniaxial tension test, two unique nonzero principal strains evolve (one is an axial strain and the other is a transverse strain), and the ratio of these two strains can be determined as it changes throughout the test. The absolute value of this ratio is the Poisson function: [6]

$$\nu(t) \equiv \left| \frac{\varepsilon_t}{\varepsilon_a} \right| \quad (1)$$

Here $\nu(t)$ is the Poisson function, ε_t is the transverse strain, and ε_a is the axial strain. This function is defined for all types of isotropic elastic behavior (including nonlinear elastic and viscoelastic). Although this ratio varies throughout the test, it can be extrapolated back to the zero deformation state (i.e., at the start of the test, when the axial strain vanishes):

$$\nu_0 = \lim_{\varepsilon_a, \varepsilon_t \rightarrow 0} \nu(\varepsilon_a, \varepsilon_t) \quad (2)$$

This limiting value is Poisson's ratio, and is related to the compressibility of the material. In the special case of a linear elastic material, the ratio is a constant value, and extrapolation is unnecessary. For each of the tests conducted here, we measured the two strains versus time, took their ratio as shown in Equation 1, and plotted that as a function of the axial strain – a typical plot is shown in Figure 3 below. For each of these datasets, a polynomial curve fit was used to determine the value for Poisson's ratio – a least-squares method was used to derive the polynomial coefficients, then ν_0 was taken to be the polynomial value when $\varepsilon_a = 0$. By varying both the temperature and strain rate in the tests, we hoped to gain insight into how Poisson's ratio varied in a complex, viscoelastic material. It now appears, however, that neither the temperature nor the strain rate significantly affect Poisson's ratio in any of the propellants that we investigated. Table 2 and 3 show the results for both the double-base and the composite propellant, respectively, when Poisson's ratio was extrapolated in this way.

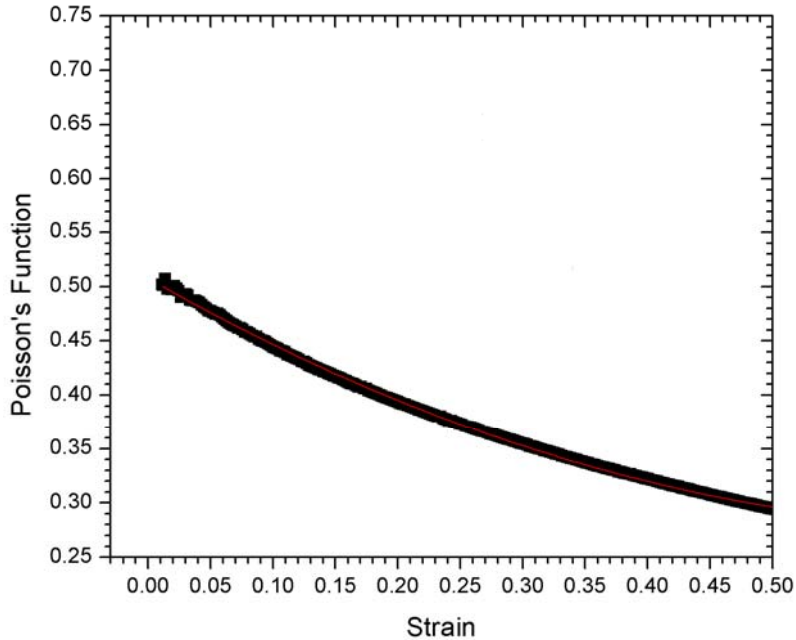


Figure 3 -- The Poisson function versus axial strain in a tensile test of a double-base propellant. The data was fit with a quadratic polynomial (shown as the thin red line in the figure).

Due to the nature of propellant and testing in general, some variance in values is likely, and this is indicated in the two tables. We think that most of this variance is due to the extrapolative nature of the analysis, although specimen-to-specimen property variations are also significant. In any case, the differences can be treated statistically by posing two alternate hypotheses. The first (the null hypothesis) stipulates that all of the values have a single mean, regardless of test condition, for a given propellant. The second hypothesis (the alternate hypothesis) stipulates that each test condition has its own unique mean. Statistical testing using an analysis of variance test (a two-parameter test statistic known as the F distribution) showed that the null hypothesis could be accepted in both cases with over a 95% confidence level. This was also found to be true for two other propellants (a double-base and a composite propellant) that had been previously tested in the same manner. This combined body of work strongly suggests that over the range of relevant temperatures and strain rates, Poisson's ratio for a given propellant does not vary significantly, and can be determined without resorting to a full test matrix. The statistical analysis of the data is not given in detail here but the methodology is discussed thoroughly elsewhere. [7]

Since it seems reasonable to conclude that both double-base and composite propellants have Poisson's ratios that are not significantly affected by temperature or strain rate for the normal range of testing, all of the values from Tables 2 and 3 have been combined to give the mean and standard deviations shown in Table 4. These results confirm the incompressible nature of the two propellants, and for structural analysis, values very close to 0.5 (e.g., 0.499) would probably be the most appropriate to use. However, it should be noted that in at least one case (another very similar double-base propellant) a value significantly less than 0.5 was found, so the general conclusion that all propellants are incompressible should not be assumed.

Table 2 -- Extrapolated Poisson's ratios for the various temperatures and crosshead speeds (double-base propellant).

		Crosshead Speed (mm/min)		
		5.08	50.8	508.0
Conditioning Temperature (deg. C)	-30.0	0.5076	0.4723	0.4391
		0.4918	0.5651	0.4852
		0.4886	0.5074	0.5166
	20.0	0.5494	0.4648	0.5750
		0.5130	0.5166	0.5253
		0.4999	0.4705	0.5253
	50.0	0.4662	0.4959	0.5169
		0.5145	0.4927	0.5479
		0.5046	0.5141	0.4703

Table 3 -- Extrapolated Poisson's ratios for the various temperatures and crosshead speeds (HTPB propellant).

		Crosshead Speed (mm/min)		
		5.08	50.8	508.0
Conditioning Temperature (deg. C)	-30.0	0.4993	-	0.5210
		0.5025	0.4785	0.5349
		0.5155	0.5097	0.4925
	20.0	0.4992	0.5269	0.5509
		0.5016	0.4768	0.5407
		0.5259	0.5609	0.5499
	50.0	0.5187	0.5302	0.4999
		0.5080	0.4992	0.5306
		0.5342	0.4454	0.5162

Table 4 -- Average values for Poisson's ratio over the range of temperatures and crosshead speeds studied.

	Double-base propellant	HTPB propellant
Poisson's ratio (mean)	0.5056	0.5142
Standard deviation	0.0320	0.0256
Coefficient of variation	6.3	5.0

CONCLUSIONS

Three-dimensional digital image correlation has been used with prismatic propellant specimens to determine the surface strains on two types of propellants. Using this data, Poisson's ratio was determined at various temperatures and strain rates. Statistical analysis shows that neither the temperature nor the strain rate had a significant effect on Poisson's ratio. The method is noncontact, works with large deformations, and is proposed as one means by which the mechanical properties of solid propellants can be determined. The elastic mechanical parameter, Poisson's ratio, has particular uses, even when associated with viscoelastic materials such as solid propellants, because under certain circumstances the elastic constitutive models suffice.

For the two propellants studied, the values for Poisson's ratio were close to the normally assumed value of 0.5 for incompressible materials. However, this should be viewed with caution, since even small deviations in Poisson's ratio can greatly affect the stress analysis results (also, in some previous work we found a value significantly different from 0.5). More importantly, perhaps, even if the data indicates that the incompressibility assumption is warranted for short-term events, this is not necessarily valid for longer duration events such as for thermal cycling, or for any phenomena where propellant damage occurs. The digital image correlation method gives additional information about the contraction of the specimen throughout the entire tensile test – similar tests can be used to further characterize the mechanical properties of the material even in the viscoelastic regime.

REFERENCES

- [1] H. K. Ching, C. T. Liu and S. C. Yen, "FE Calculations of J-Integral in a Constrained Elastomeric Disc with Crack Surface Pressures," in *ASME International Mechanical Engineering Congress and Exposition*, Anaheim, California, 2004.
- [2] H. T. Chu and J. H. Chou, "Poisson Ratio Effect on Stress Behavior of Propellant Grain Under Ignition Loading," *Journal of Propulsion and Power*, vol. 27, no. 3, pp. 662-667, May-June 2011.
- [3] ASTM International, "ASTM Standard E132-04, Standard Test Method for Poisson's Ratio at Room Temperature," West Conshohocken, Pennsylvania, 2010.
- [4] R. J. Farris, "Dilatation of Granular Filled Elastomers Under High Rates of Strain," *Journal of Applied Polymer Science*, vol. 8, pp. 25-35, 1964.
- [5] M. A. Sutton, J. J. Orteu and H. Schreier, *Image Correlation for Shape, Motion and Deformation Measurements: Basic Concepts, Theory, and Applications*, New York: Springer Science + Business Media LLC, 2009.
- [6] M. F. Beatty and D. O. Stalnaker, "IMA Preprint Series #215: The Poisson Function of Finite Elasticity," Institute for Math and Its Applications, University of Minnesota, Saint Paul, Minnesota, 1986.
- [7] J. Mandel, *The Statistical Analysis of Experimental Data*, New York: Dover Publications, 1984.

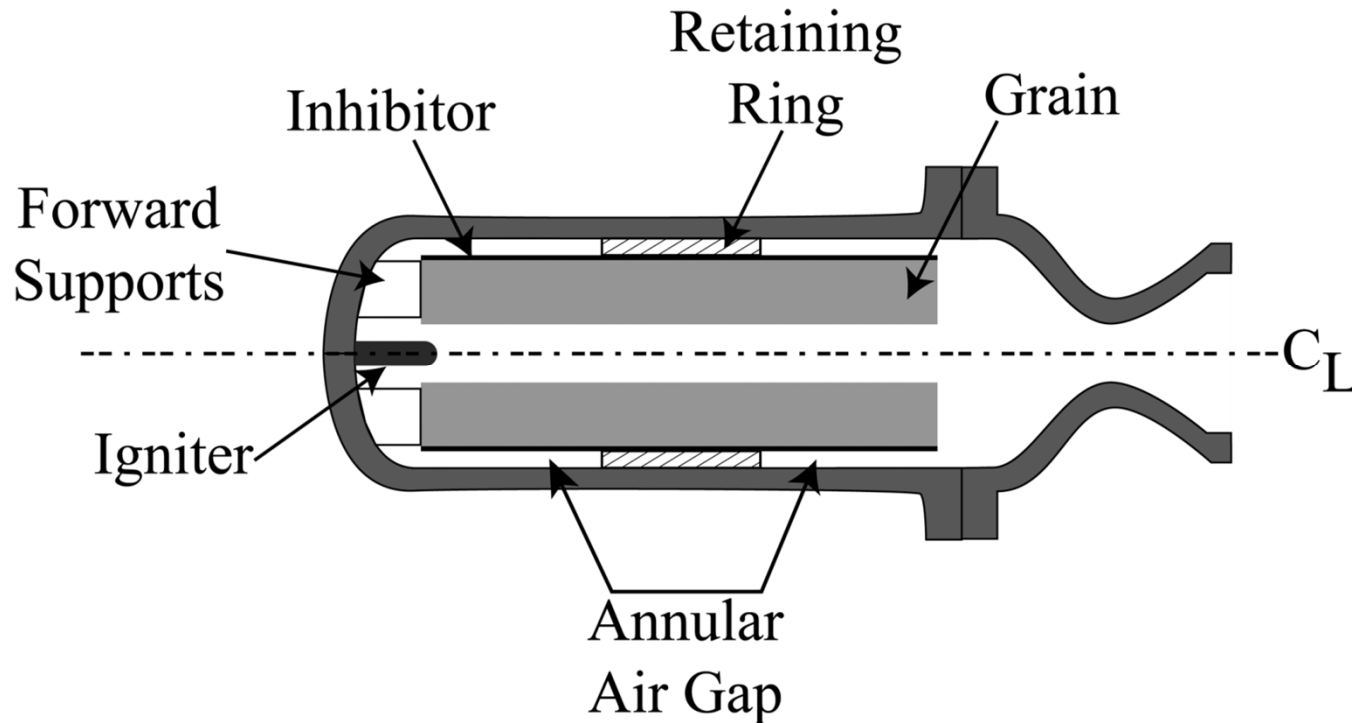


Poisson's Ratio Extrapolation from Digital Image Correlation Experiments

T. C. Miller
AFRL/RQRP
May 2013

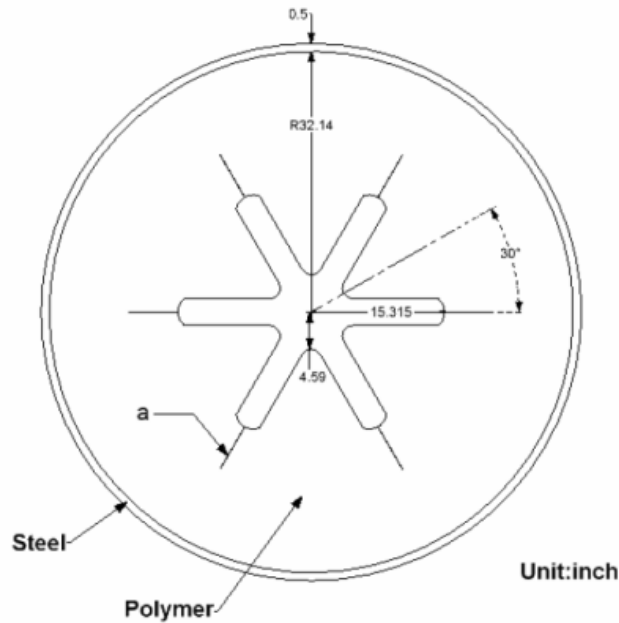


Poisson's Ratio in Propellant – Why It Matters

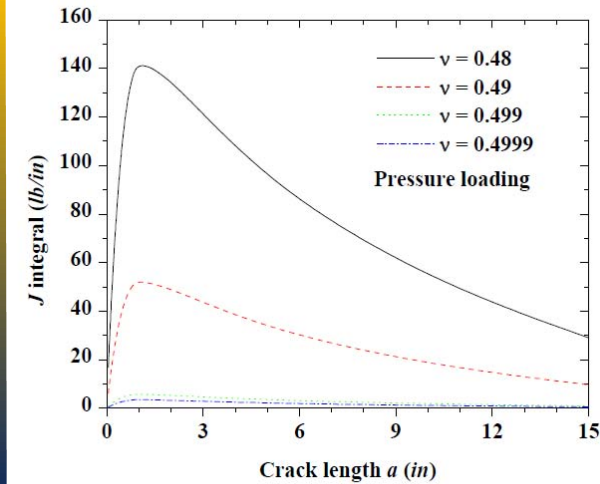
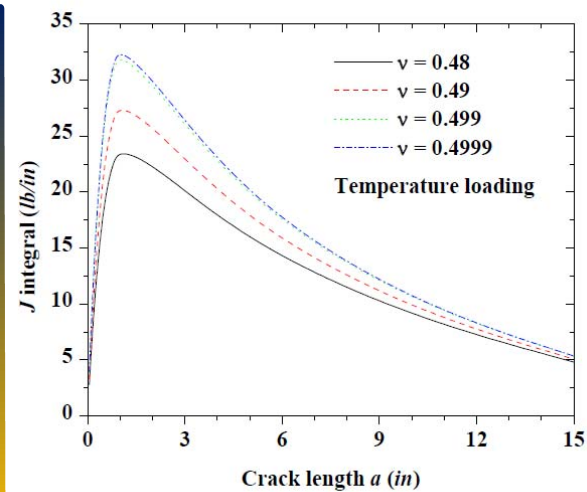




Fracture Mechanics and Poisson's Ratio



Ching, H. K., Liu, C. T., and Yen, S. C., FE Calculations of J-Integral in a Constrained Elastomeric Disc with Crack Surface Pressures and Isothermal Loads, ASME International Congress & Exposition, 13-19 November 2004, Anaheim, CA





Stress Analyses and Poisson's Ratio

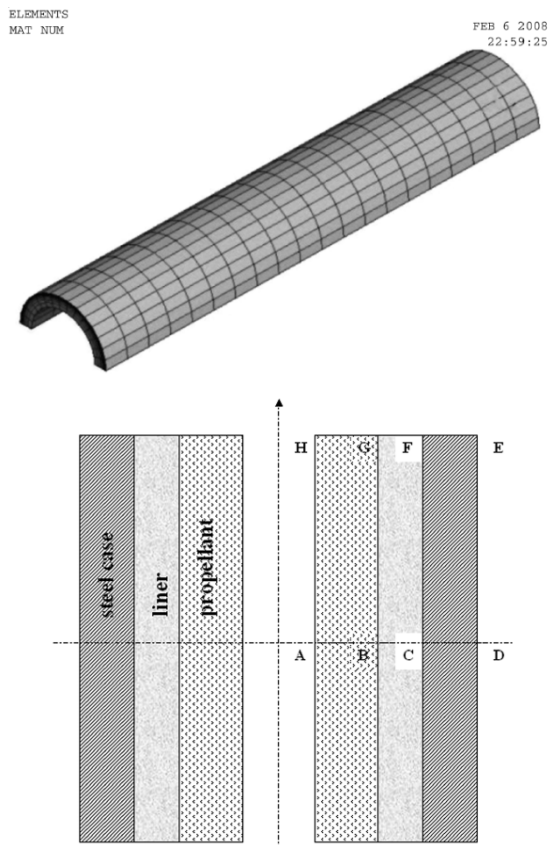
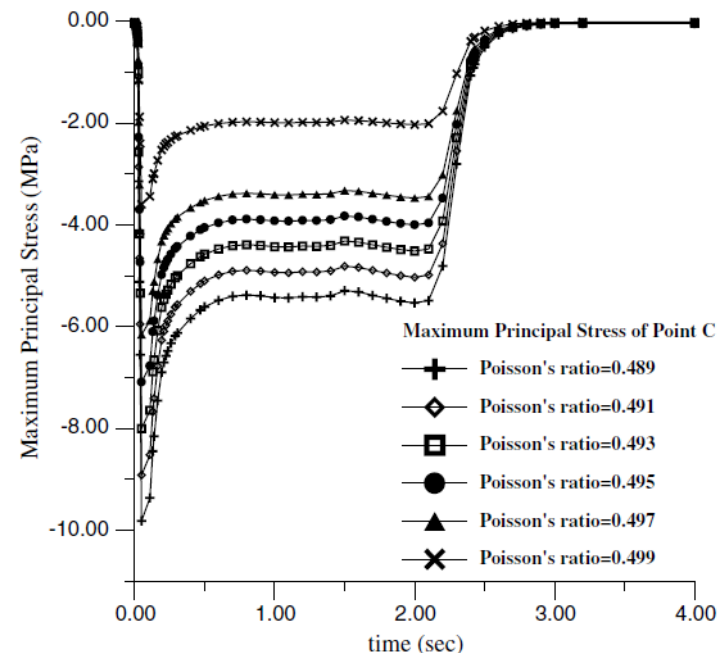


Fig. 11 Cross-sectional diagram of the SRM.

Chu, Hung-Ta and Chou, Jung-Hua, Poisson Ratio Effect on Stress Behavior of Propellant Grains Under Ignition Loading, Journal of Propulsion and Power, Vol 27, No. 3, May-June 2011.



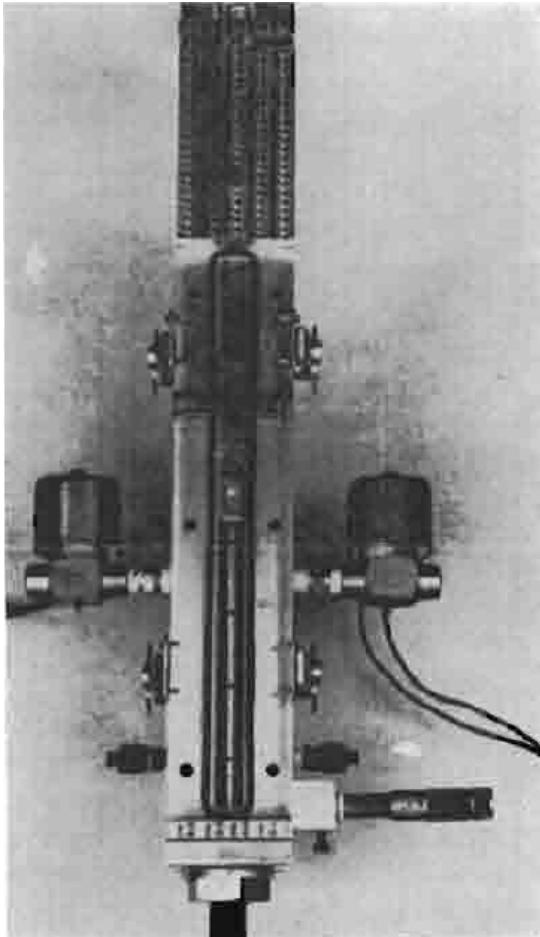
“Conventionally, the value of solid propellant grains is assumed to be a constant to simplify the experimental task, but the real value is from 0.48 to 0.499, depending on the chemical design of the solid propellant grains. In this study, results show that the Poisson ratio variation effect is very important for the structural integrity of solid propellant grains”... “Therefore, unlike metallic structures, an exact value of the Poisson ratio for polymer materials is very important, and an improper assumption may cause the structural integrity of a missile system subjected to pressure loading to be wrongly evaluated.”



Measurements of Poisson's Ratio in Solid Propellants – State of the Art





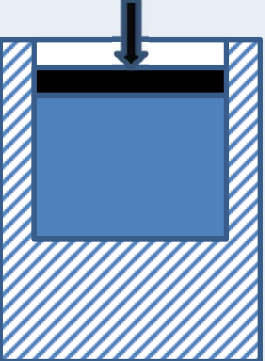
(R. J. Farris' dilatometer)



- Enclose a constant volume of gas in a container along with the specimen
- Equilibrate everything to the temperature of interest
- Measure the pressure of the gas at the start of the test
- Measure the pressure of the gas during the test, when it is expanding ever so slightly due to the very slight compressibility of the specimen
- Use crosshead motion of specimen inside dilatometer to get E
- Combine results (Use E & K to get Poisson's ratio)



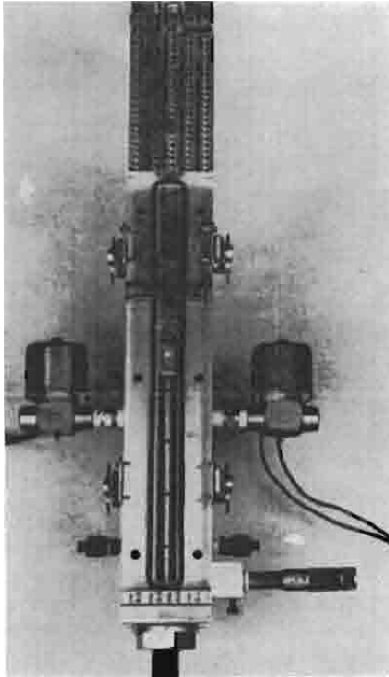
Poisson's Ratio

Parameter	E	ν_0	μ	K
Associated Test				

	(K, E)	(K, μ)	(K, ν_0)	(E, μ)	(E, ν_0)	(μ , ν_0)
K =	K	K	K	$\frac{E\mu}{3(3\mu - E)}$	$\frac{E}{3(1 - 2\nu_0)}$	$\frac{2\mu(1 + \nu_0)}{3(1 - 2\nu_0)}$
E =	E	$\frac{9K\mu}{3K + \mu}$	$3K(1 - 2\nu_0)$	E	E	$2\mu(1 + \nu_0)$
μ =	$\frac{3KE}{9K - E}$	μ	$\frac{3K(1 - 2\nu_0)}{2(1 + \nu_0)}$	μ	$\frac{E}{2(1 + \nu_0)}$	μ
ν_0 =	$\frac{3K - E}{6K}$	$\frac{3K - 2\mu}{2(3K + \mu)}$	ν_0	$\frac{E}{2\mu} - 1$	ν_0	ν_0



Dilatometer Measurements and Uncertainty Analysis



$$\nu_0 = \frac{3K - E}{6K} = \frac{1}{2} - \frac{E}{6K}$$

$$f = \frac{ab...c}{xy...z}$$

$$\frac{\Delta f}{f} = \sqrt{\left(\frac{\Delta a}{a}\right)^2 + \left(\frac{\Delta b}{b}\right)^2 + \dots + \left(\frac{\Delta x}{x}\right)^2 + \left(\frac{\Delta y}{y}\right)^2 + \dots + \left(\frac{\Delta z}{z}\right)^2}$$

$$\frac{\Delta \nu_0}{\nu_0} = \sqrt{\left(\frac{\Delta K}{K}\right)^2 + \left(\frac{\Delta E}{E}\right)^2}$$

Poisson's ratio as a function of Young's modulus and bulk modulus

...a generic ratio of two products

...the relation between all of the coefficients of variation

...the result (propagation of errors for a Farris dilatometer)

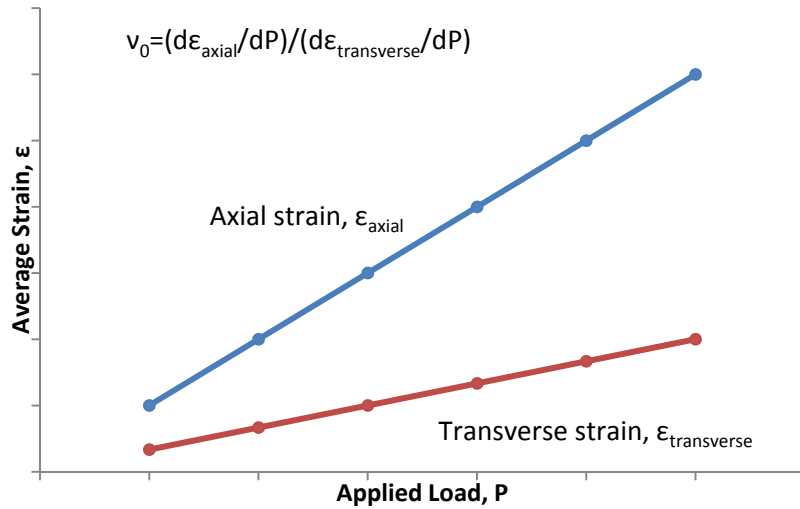
...Recent analysis of data on Young's modulus for four pint batches of propellant gave coefficient of variation of slightly less than 5%.

Parameter:	Nominal Value:	CV
K:	200,000	5.00%
E:	1,000	5.00%
ν_0 :	0.4992	7.07%

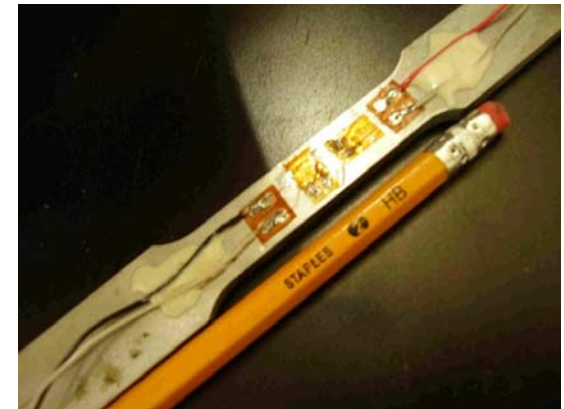
“The determination of $K(t)$ from $E(t)$ and $G(t)$ thus resembles the attempt to determine the weight of the captain by weighing the ship with and without him.” (N.W. Tschoegl, N. W., Knauss, Wolfgang G., and Emri, Igor, Poisson's Ratio in Linear Viscoelasticity – A Critical Review, *Mechanics of Time-Dependent Materials* 6: 3–51, 2002)



Measurement of Poisson's Ratio in Linear Elastic Materials

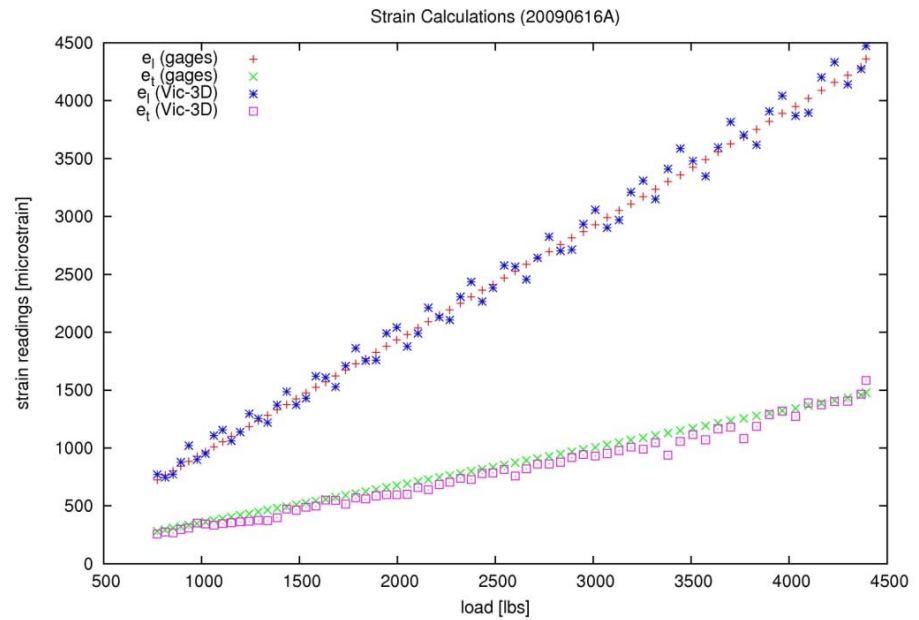


(From ASTM E132-86)





Measurement of Poisson's Ratio in Linear Elastic Materials





Measurement of Poisson's Ratio in Linear Elastic Materials



Method	Poisson's ratio value	Coefficient of Variation (%)
Book value	0.330	N/A
Strain gauges	0.324	1.95
Imaging system	0.328	1.98

Fine												Coarse											
Near						Far						Near						Far					
N=6			N=12			N=6			N=12			N=6			N=12			N=6			N=12		
1	2	3	4	5	6	7	8	9	10	11	12	13	14	15	16	17	18	19	20	21	22	23	24



Digital Image Correlation Concepts

$$r_{ij} = \frac{\sum_{i=1}^n \sum_{j=1}^n (F_{ij} - \bar{F}_{ij})^2}{\sum_{i=1}^n \sum_{j=1}^n (F_{ij} - F_{avg})^2 + \sum_{i=1}^n \sum_{j=1}^n (\bar{F}_{ij} - \bar{F}_{avg})^2}$$

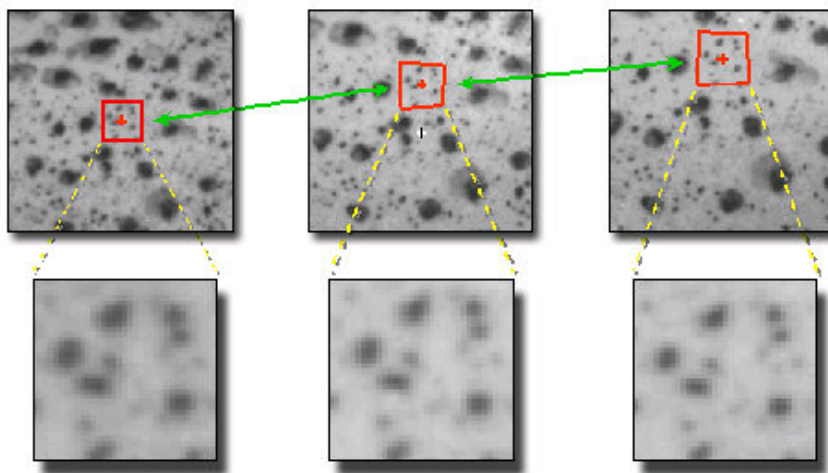
255	254	253	220	167	154	232	255	254
240	242	232	185	165	152	254	247	255
X	X	X	X	X	X	X	X	X
X	X	X	X	X	X	X	X	X
X	X	X	X	X	X	X	X	X
X	X	X	X	X	X	X	X	X
X	X	X	X	X	X	X	X	X
X	X	X	X	X	X	X	X	X
X	X	X	X	X	X	X	X	X
X	X	X	X	X	X	X	X	X

255	254	253	220	167	154	232	255	254
240	242	232	185	165	152	254	247	255
X	X	X	X	X	X	X	X	X
X	X	X	X	X	X	X	X	X
X	X	X	X	X	X	X	X	X
X	X	X	X	X	X	X	X	X
X	X	X	X	X	X	X	X	X
X	X	X	X	X	X	X	X	X
X	X	X	X	X	X	X	X	X
X	X	X	X	X	X	X	X	X

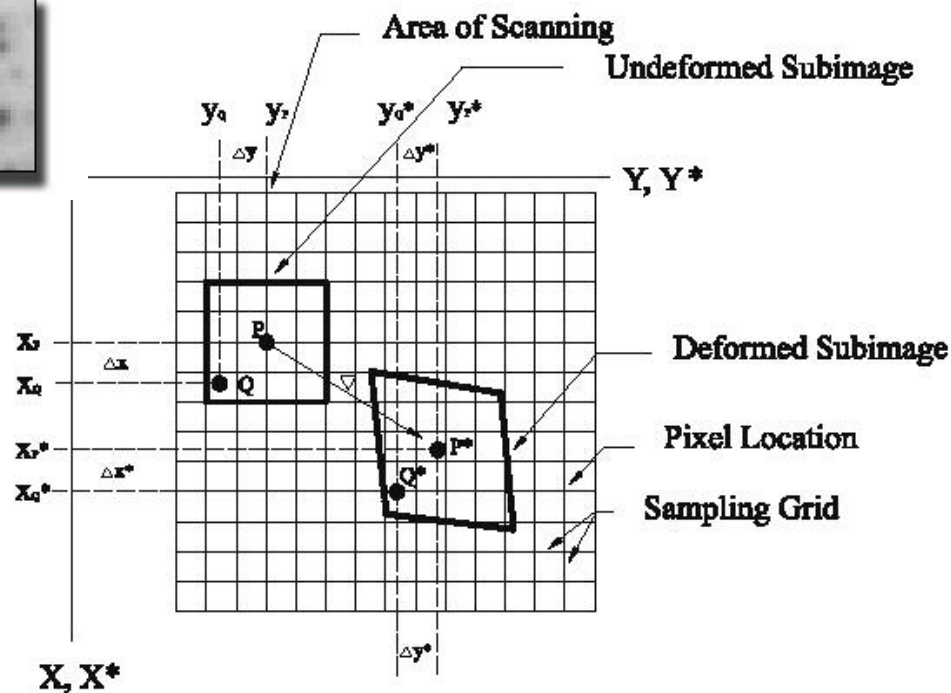
$$r_{ij} = 1 - \frac{\sum_{i=1}^n \sum_{j=1}^n (F_{ij} - F_{avg})(\bar{F}_{ij} - \bar{F}_{avg})}{\sqrt{\sum_{i=1}^n \sum_{j=1}^n (F_{ij} - F_{avg})^2 + \sum_{i=1}^n \sum_{j=1}^n (\bar{F}_{ij} - \bar{F}_{avg})^2}}$$



Digital Image Correlation Concepts



$$\bar{x} = x + \frac{\partial u}{\partial x} \Delta x + \frac{\partial u}{\partial y} \Delta y$$



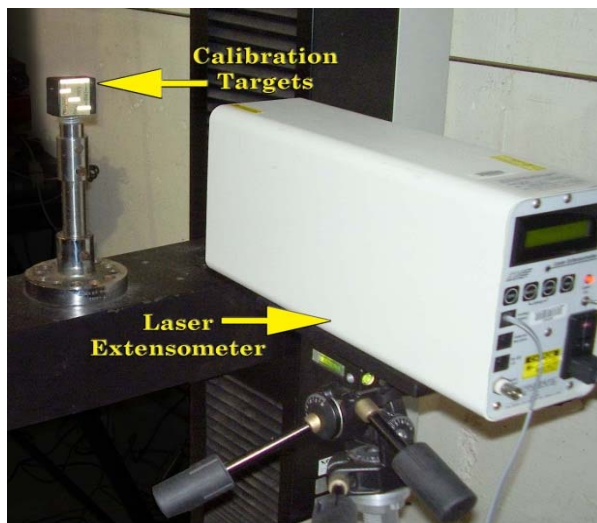
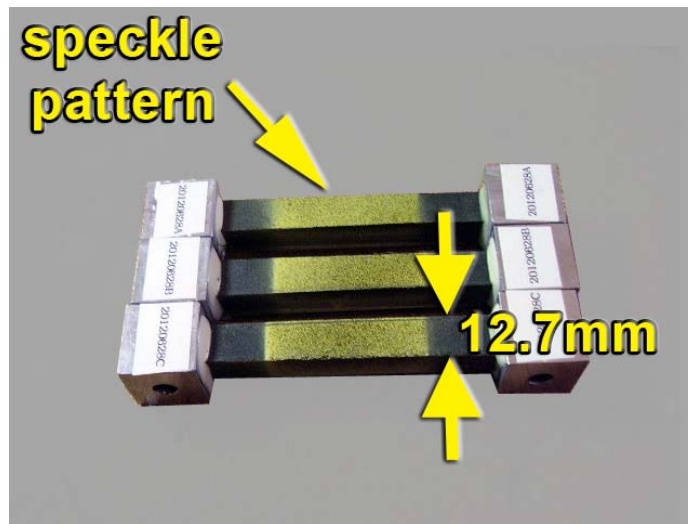


Analogous Work on Solid Propellants





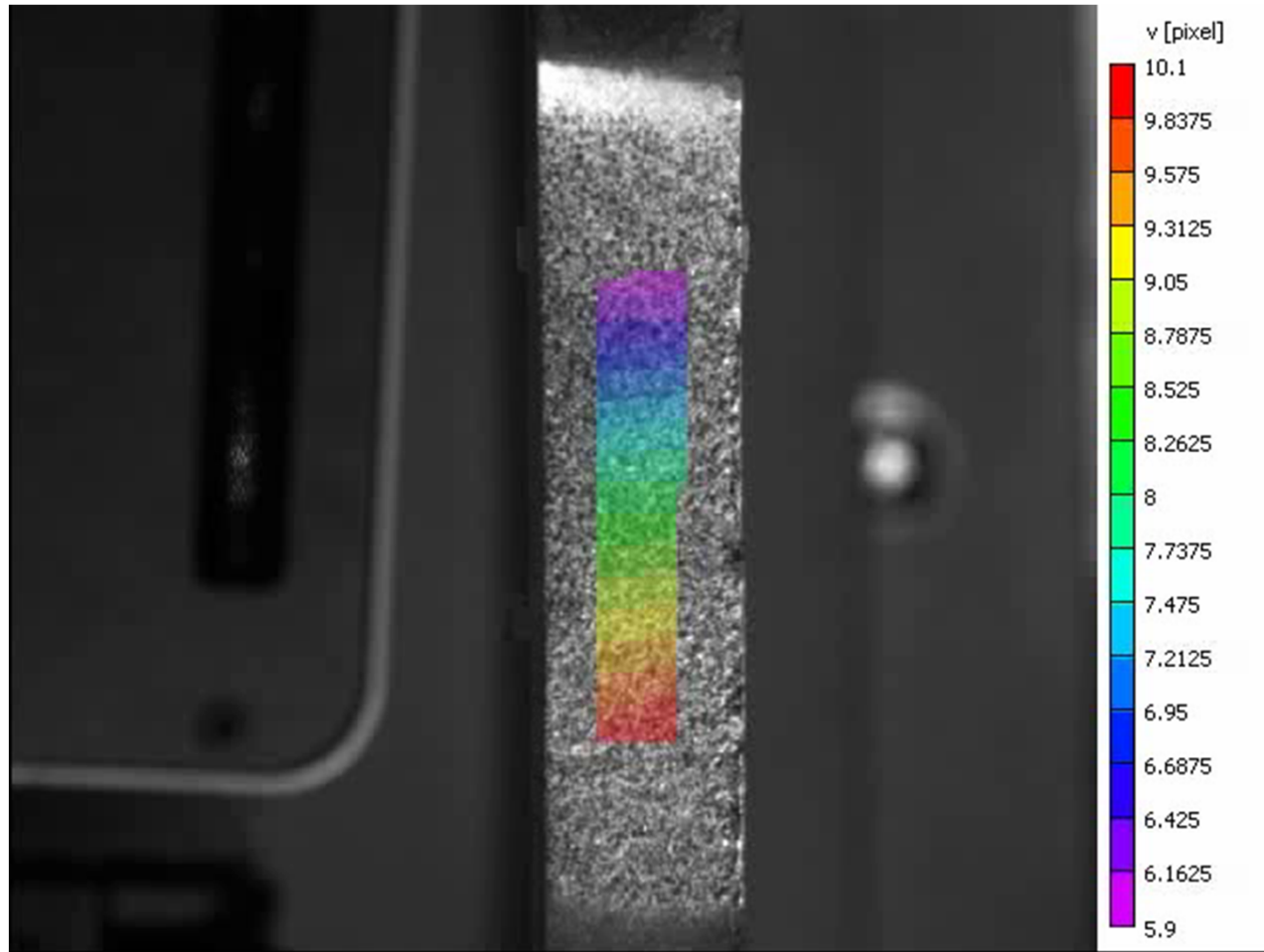
Experimental Techniques





Damage Characterization of Propellants

Video of Three-Dimensional Image Correlation Method Applied to Titan IV Propellant

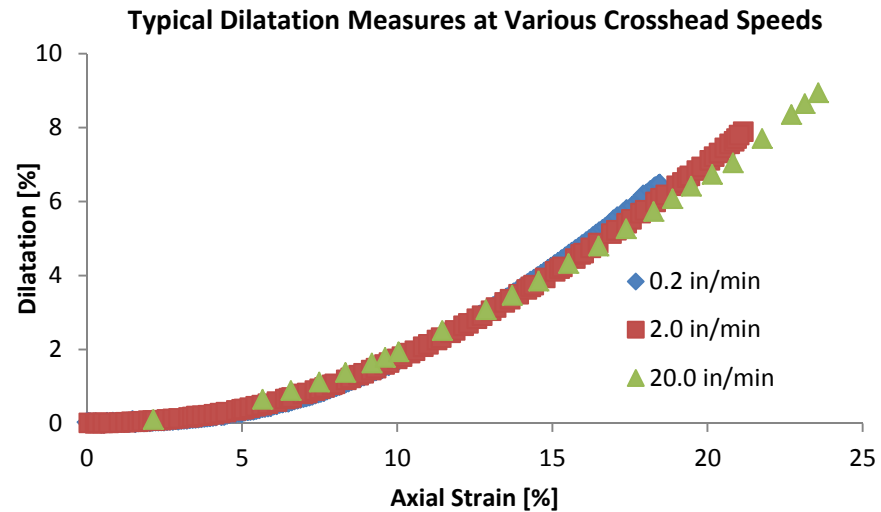
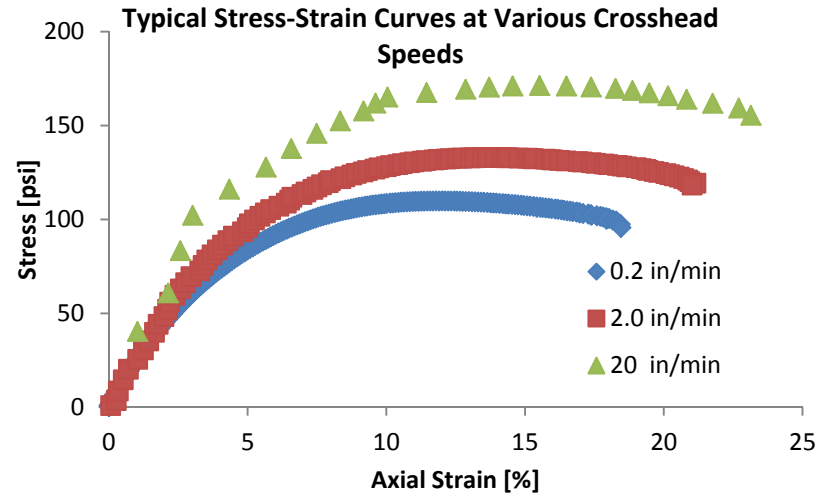




Damage Characterization of Propellants



Dewetting Results





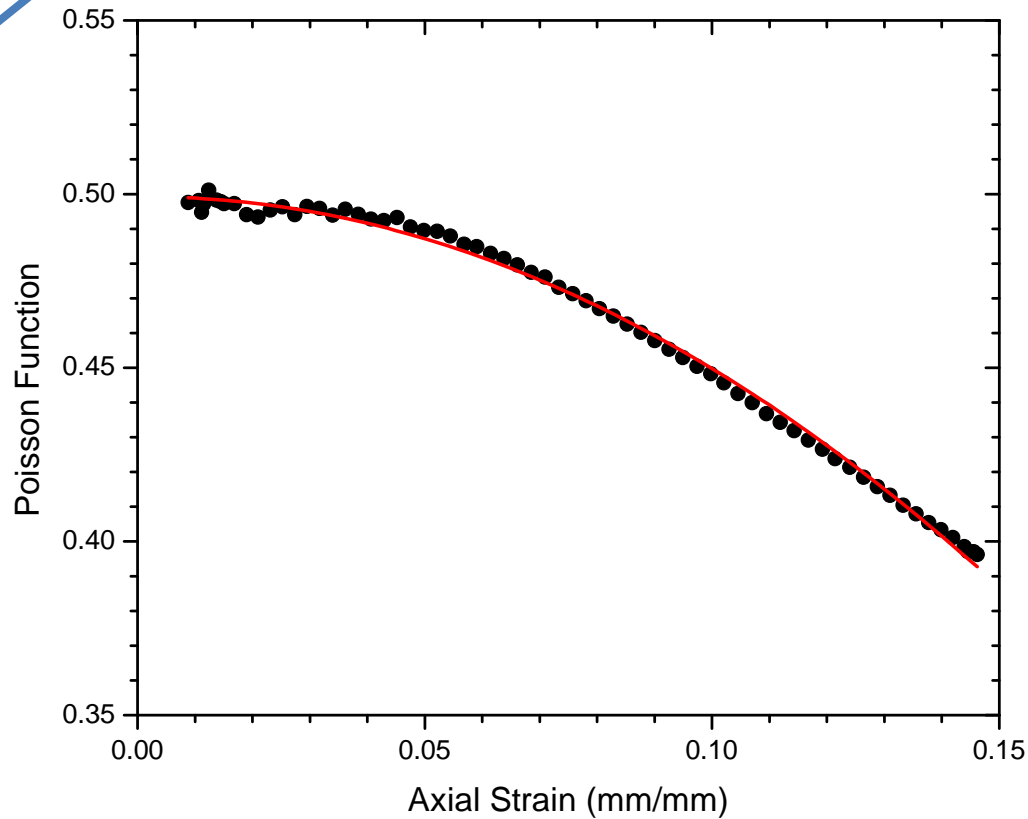
Damage Characterization of Propellants

Poisson's Ratio Results (Typical Extrapolation)



Poisson Function	Poisson's Ratio
$\nu(t) = \left \frac{\epsilon_{axial}}{\epsilon_{transverse}} \right $	$\nu_0 = \lim_{\epsilon_{axial} \rightarrow 0} \nu(t)$

Constant for a linear elastic material, but not so for more complex materials

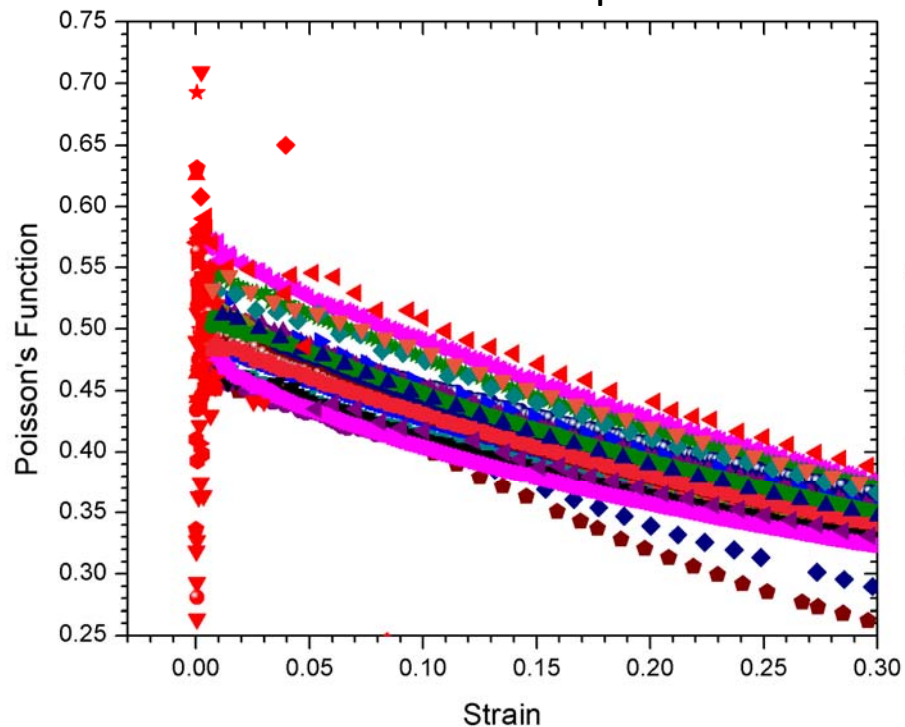




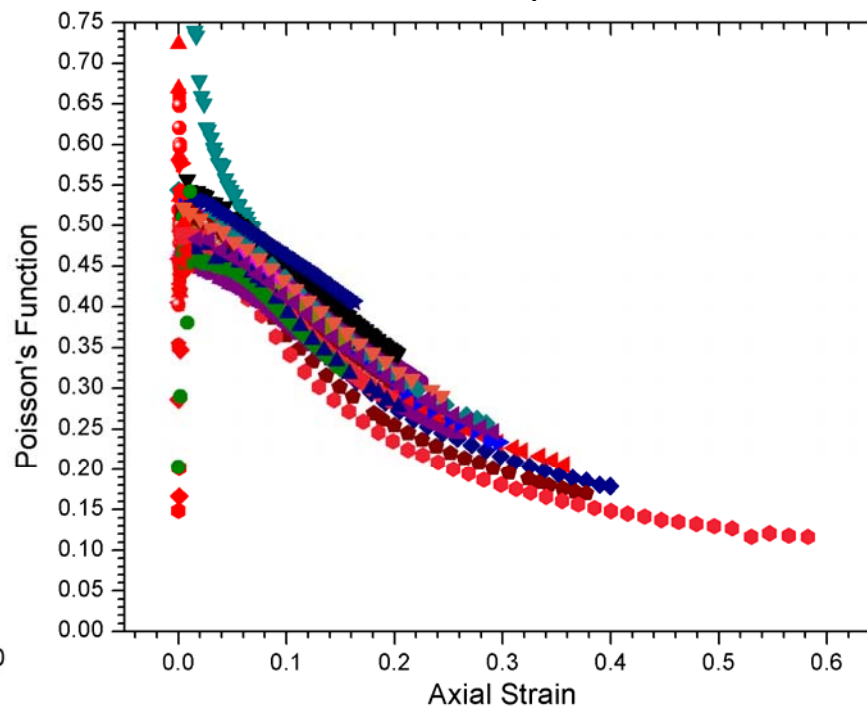
Data from Both Propellants



Double-Base Propellant



HTPB Propellant





Poisson's Ratio Results

Double-Base Propellant

		Crosshead Speed (mm/min)		
		5.08	50.8	508.0
Conditioning Temperature (deg. C)	-30.0	0.5076	0.4723	0.4391
		0.4918	0.5651	0.4852
		0.4886	0.5074	0.5166
	20.0	0.5494	0.4648	0.5750
		0.5130	0.5166	0.5253
		0.4999	0.4705	0.5253
	50.0	0.4662	0.4959	0.5169
		0.5145	0.4927	0.5479
		0.5046	0.5141	0.4703

HTPB Propellant

		Crosshead Speed (mm/min)		
		5.08	50.8	508.0
Conditioning Temperature (deg. C)	-30.0	0.4993	-	0.5210
		0.5025	0.4785	0.5349
		0.5155	0.5097	0.4925
	20.0	0.4992	0.5269	0.5509
		0.5016	0.4768	0.5407
		0.5259	0.5609	0.5499
	50.0	0.5187	0.5302	0.4999
		0.5080	0.4992	0.5306
		0.5342	0.4454	0.5162



Effects of Temperature and Strain Rate – Statistical Tests



HTPB Propellant Analysis of Variance									
i	j	Model I (a single average)				Model II (distinct averages)			
		vij	avg	dij	squared	vij	avg	dij	squared
1	1	0.4993	0.5142	-0.0149	2.2190E-04	0.4993	0.5058	-0.0065	4.1818E-05
1	2	0.5025	0.5142	-0.0117	1.3680E-04	0.5025	0.5058	-0.0033	1.0671E-05
1	3	0.5155	0.5142	0.0013	1.7000E-06	0.5155	0.5058	0.0097	9.4738E-05
2	1	0.4785	0.5142	-0.0357	1.2742E-03	0.4785	0.4941	-0.0156	2.4336E-04
2	2	0.5097	0.5142	-0.0045	2.0215E-05	0.5097	0.4941	0.0156	2.4336E-04
3	1	0.5210	0.5142	0.0068	4.6292E-05	0.5210	0.5161	0.0049	2.3684E-05
3	2	0.5349	0.5142	0.0207	4.2865E-04	0.5349	0.5161	0.0188	3.5219E-04
3	3	0.4925	0.5142	-0.0217	4.7072E-04	0.4925	0.5161	-0.0236	5.5853E-04
4	1	0.4992	0.5142	-0.0150	2.2488E-04	0.4992	0.5089	-0.0097	9.4090E-05
4	2	0.5016	0.5142	-0.0126	1.5866E-04	0.5016	0.5089	-0.0073	5.3290E-05
4	3	0.5259	0.5142	0.0117	1.3698E-04	0.5259	0.5089	0.0170	2.8900E-04
5	1	0.5269	0.5142	0.0127	1.6139E-04	0.5269	0.5215	0.0054	2.8801E-05
5	2	0.4768	0.5142	-0.0374	1.3985E-03	0.4768	0.5215	-0.0447	2.0011E-03
5	3	0.5609	0.5142	0.0467	2.1812E-03	0.5609	0.5215	0.0394	1.5497E-03
6	1	0.5509	0.5142	0.0367	1.3472E-03	0.5509	0.5472	0.0037	1.3938E-05
6	2	0.5407	0.5142	0.0265	7.0245E-04	0.5407	0.5472	-0.0065	4.1818E-05
6	3	0.5499	0.5142	0.0357	1.2748E-03	0.5499	0.5472	0.0027	7.4711E-06
7	1	0.5187	0.5142	0.0045	2.0285E-05	0.5187	0.5203	-0.0016	2.5600E-06
7	2	0.5080	0.5142	-0.0062	3.8392E-05	0.5080	0.5203	-0.0123	1.5129E-04
7	3	0.5342	0.5142	0.0200	4.0015E-04	0.5342	0.5203	0.0139	1.9321E-04
8	1	0.5302	0.5142	0.0160	2.5612E-04	0.5302	0.4916	0.0386	1.4900E-03
8	2	0.4992	0.5142	-0.0150	2.2488E-04	0.4992	0.4916	0.0076	5.7760E-05
8	3	0.4454	0.5142	-0.0688	4.7329E-03	0.4454	0.4916	-0.0462	2.1344E-03
9	1	0.4999	0.5142	-0.0143	2.0438E-04	0.4999	0.5156	-0.0157	2.4544E-04
9	2	0.5306	0.5142	0.0164	2.6909E-04	0.5306	0.5156	0.0150	2.2600E-04
9	3	0.5162	0.5142	0.0020	4.0154E-06	0.5162	0.5156	0.0006	4.0111E-07

Model I:	$(v_0)_{ij} = \mu + \epsilon_{ij}$	Model II:	$(v_0)_{ij} = \mu_i + \epsilon_{ij}$
----------	------------------------------------	-----------	--------------------------------------

Model	dof	SS	MS
I	25	SS _I = 1.6337E-02	MS _I = 6.5347E-04
II	17	SS _{II} = 1.0149E-02	MS _{II} = 5.9698E-04
Difference	8	SS _{III} = 6.1881E-03	MS _{III} = 7.7351E-04

$F_{8,17} = \frac{MS_{III}}{MS_{II}} = \frac{7.7351E-4}{5.9698E-4} = 1.29$	$F_{crit} = 2.548 (\alpha = 0.05)$
--	------------------------------------

Distribution A: Approved for public release; distribution unlimited. Public Affairs Clearance Number XXXXX.



Damage Characterization of Propellants

Poisson's Ratio Results (Average Values)



	Inert HTPB propellant	First double-base propellant	Second double-base propellant	HTPB propellant
Poisson's ratio (mean)	0.4992	0.4864	0.5056	0.5142
Standard deviation	0.0102	0.0117	0.0320	0.0256
Coefficient of variation	2.1%	2.4%	6.3%	5.0%



Summary and Conclusions

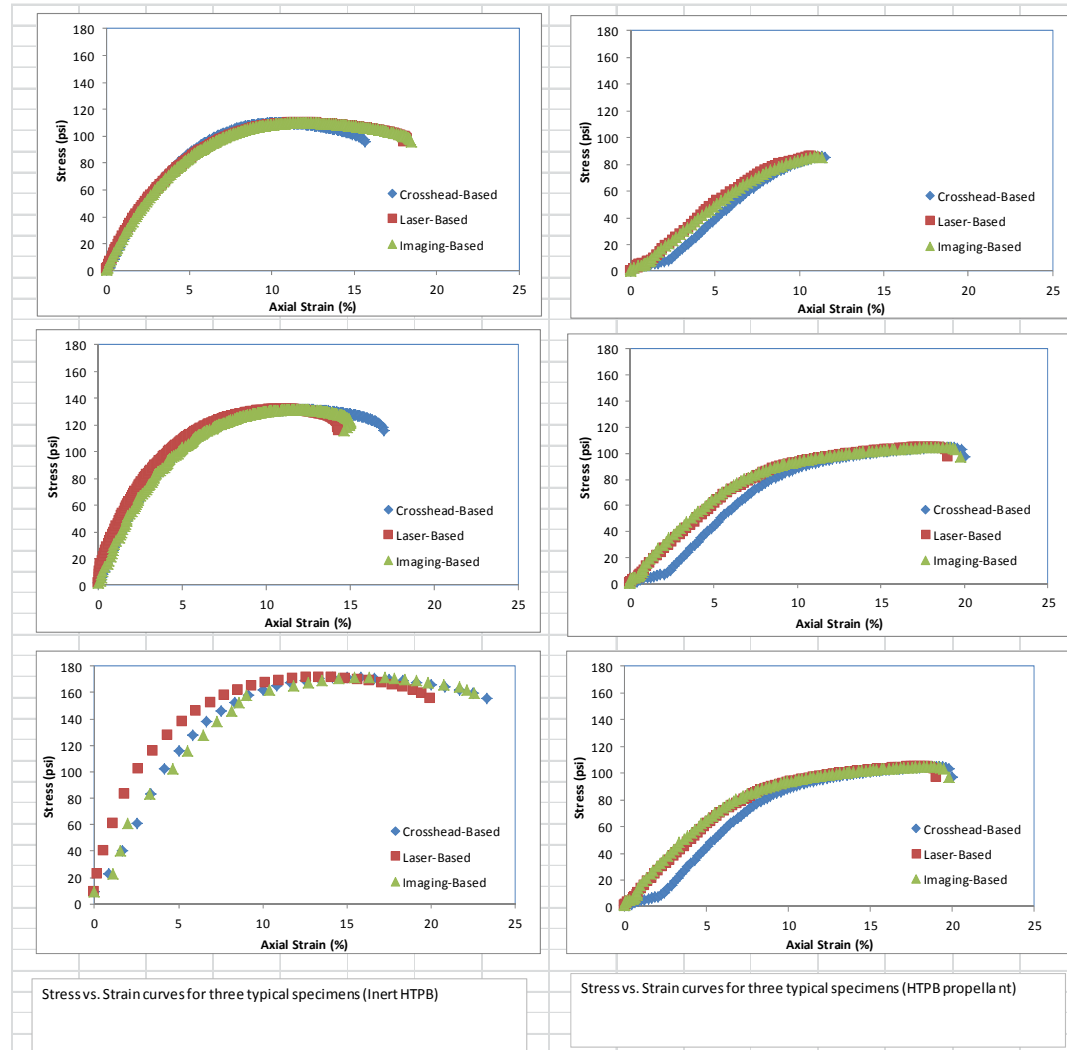
- Digital image correlation can be used to get volume change information with solid propellants – this volume change data can be extrapolated to get Poisson's ratio.
- Over the ranges considered, Poisson's ratio does not seem to vary significantly with temperature or strain rate.
- This method has accuracies comparable to existing methods and is noncontact method that does not require immersion of the specimen in a fluid or any enclosing chamber during testing.
- The digital image correlation method, because of its full-field nature, large-strain capabilities, and ease of use, has advantages for other experimental studies involving solid propellants.
- Although the data generally indicate that the incompressibility assumption is valid, in at least one case this was not warranted – additional testing on propellants is needed to verify or ensure structural analyses of motor grains.



Backup Slides

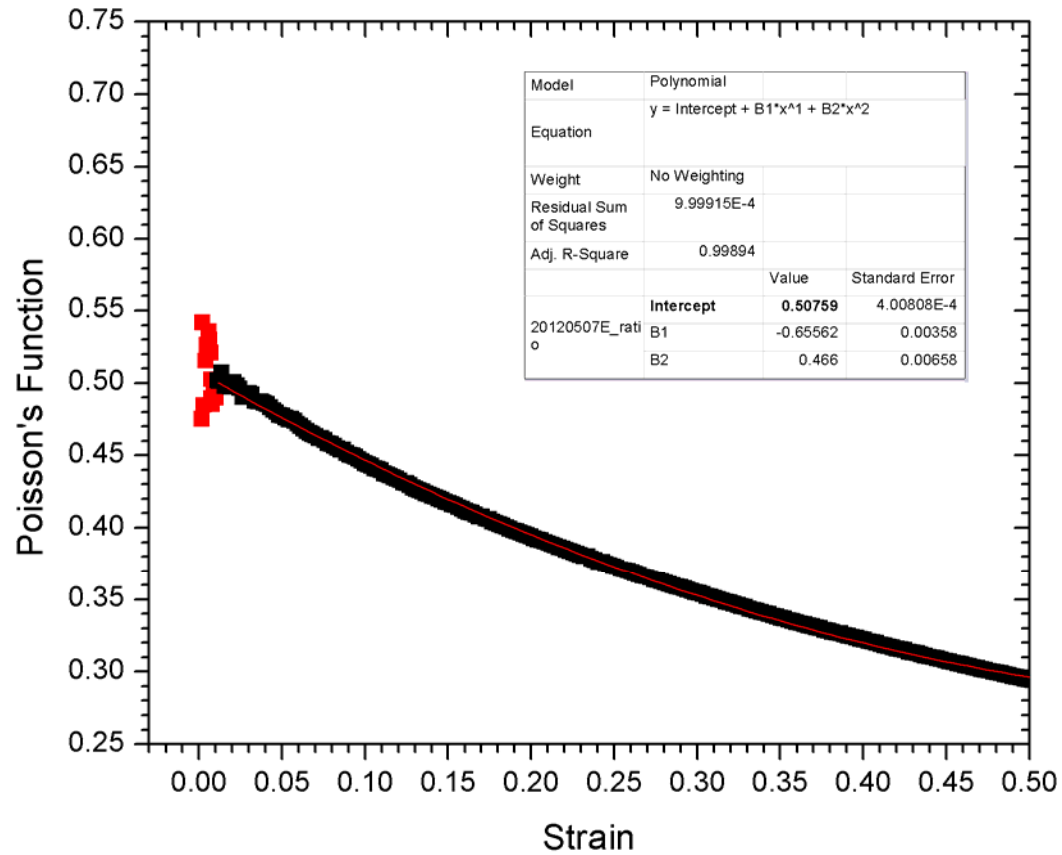


Axial Strain Comparisons





Extrapolation of Poisson's Ratio from the Poisson function





Noise Levels and Extrapolation



When two functions both approach zero as you go towards a limit, what is the limit of the ratio?

$$f(x) = 6x^2 - 2x$$

$$g(x) = 16x^2 - 4x$$

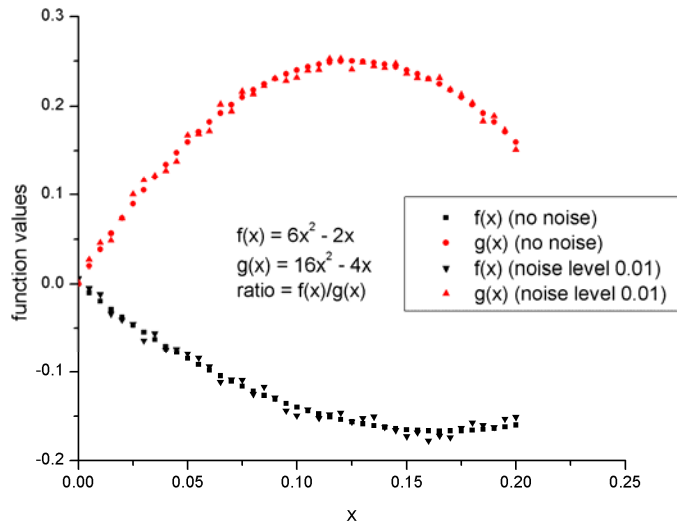
$$\lim_{x \rightarrow 0} f(x) = 0$$

$$\lim_{x \rightarrow 0} g(x) = 0$$

$$\lim_{x \rightarrow 0} \frac{f(x)}{g(x)} = \lim_{x \rightarrow 0} \frac{0}{0} = ?$$

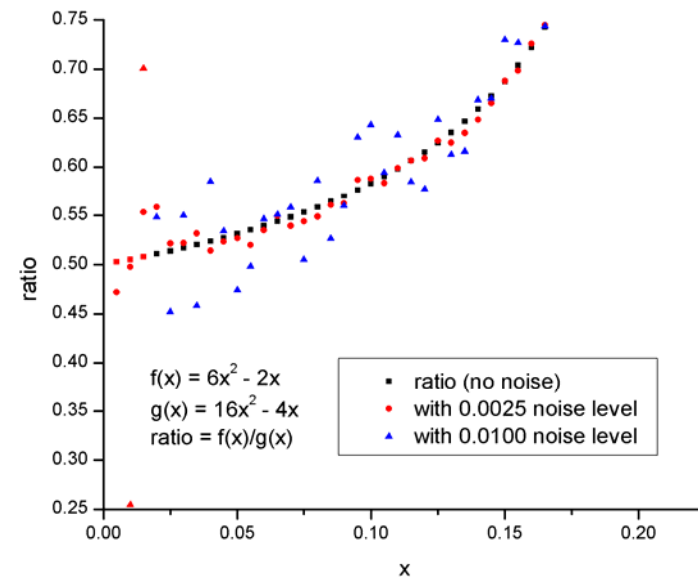
You have to use L'Hôpital's Rule:

$$\lim_{x \rightarrow 0} \frac{f(x)}{g(x)} = \lim_{x \rightarrow 0} \frac{f'(x)}{g'(x)} = \lim_{x \rightarrow 0} \frac{12x - 2}{32x - 4} = \frac{1}{2}$$



With real data (data with noise), as the two numbers in the ratio both approach zero, the noise becomes the dominant aspect of the data.

Explained another way: Small levels of noise in the numerator and denominator of a fraction become hugely important when the numerator and denominator are both small.



Moral: Expect larger variations in ratios like this when you get close to the limit.

Unless you're extrapolating with data that exists only near this limit, however, this shouldn't strongly affect the final value of the extrapolation.